Oscillation Control of Two-Wheeled Robot using a Gyrostabilizer

Faruk ÜNKER[1],* iD

[1]Gümüşhane University Faculty of Engineering and Natural Sciences, Department of Mechanical Engineerings, 29100, Bağlarbaşı/GÜMÜŞHANE

Abstract

Two-wheeled robots are popular in transportation applications because of their high manoeuvrability. In this research, the oscillation attenuation performance of the control moment gyroscope (CMG) for the two-wheeled robot was studied. This CMG is also more reactionless than other conventional absorbers by transforming the impact of angular momentum to unidirectional thrust along the center of gravity. The gimbals can precess while providing the angular momentum under the gravitational force. The CMG to be used for balancing the robot can maintain its stability in the desired frequency band. Because increasing the flywheel speed can produce the thrust force much more easily against the undesired oscillation forces that disrupt the balance of the robot. There is a relation between the gimbal amplitude and the flywheel speed of CMG, in which the required flywheel speed can be reduced if the higher gimbal amplitude is chosen. It can be also concluded from the study that the oscillation amplitudes at the target frequency can decrease as much as flywheel speed increases. There was also a mathematical model using ANSYS software. The simulation results using ANSYS matched well with the theoretical results of the Lagrangian model.

1. INTRODUCTION

Due to their high maneuverability, two-wheeled robots are popular in transportation applications (http://segway.com) despite the stability problem of an inverted pendulum [1]. The stability of the inverted pendulum-like robot has attracted significant interest over the past years [2,3]. There are apparent techniques for both the dynamics and control of these robots. An inverted pendulum-like robot is an unstable nonlinear vehicle that strongly depends on the center of gravity. [4,5]. However, two-wheeled robots can be balanced with appropriate control despite their being naturally unstable. For the sake of example, moving the wheel(s) of the robot [6,7], exerting a gyroscopic moment (CMG) [1], and riding a reaction wheel [8]. A common control strategy is to turn the wheels of the robot to move the center of a body mass forward and rear respectively. A two-wheeled robot requires a roll angle to be able to control the robot's balance under certain conditions such as the inertia forces of gravity, which significantly reduces its mobility in the upright position. Therefore, maintaining the equilibrium of forces brings interesting challenges to the researchers discussing different more realistic dynamical models to stabilize robots [4-8].

A reaction wheel is a simple and low-cost momentum actuator that can produce torque to balance the robot in the absence of ground reaction [8]. However, a primary challenge in conventional reaction wheels is that they have to change flywheel velocity to generate angular momentum to compensate the robot against constant falling-down force, which results in low momentum storage capacity. This is the main problem of reaction wheels that limits their application when the body mass is subject to continuous roll disturbances. However, compared with reaction wheels, a CMG is able to produce large amounts of torque per unit mass against continuous moments using a constant flywheel velocity. In recent years,

various studies have shown that the inertial forces of a structure can be controlled reactionless by using the gyroscopic torque produced by a rotating flywheel [9-11].

In this paper, the vibration attenuation performance of a CMG for a two-wheeled robot (an inverted pendulum problem) is investigated under the harmonic excitation torque of wheels. The angular momentum of a gyroscope stabilizer can provide weight and volume savings and ground-independent damping compared to conventional vibration absorbers [9-11]. Conventional vibration dampers generally operate on the principle of energy transfer from the main structure to the damper in the low frequency band [12]. However, the gyroscope can oscillate and precess while converting the angular momentum to linear along the center of body mass under the gravitational force within a wide range of excitation frequencies [9-11].

2. OVERVIEW OF ROBOT

Sinusoidal driving torque of $\tau = \tau_0 \cos(\omega t)$ is applied to the robot wheels using forcing amplitudes (τ_0) and different forcing frequencies (ω). Table 1 gives the technical parameters of the robot model. Gyroscopes consist of a flywheel, which is assumed to have a certain rotational speed Ω, inside a gimbal that can rotate (θ) freely around its geometric axis in the body of the robot, as shown in Figures 1 and 2.
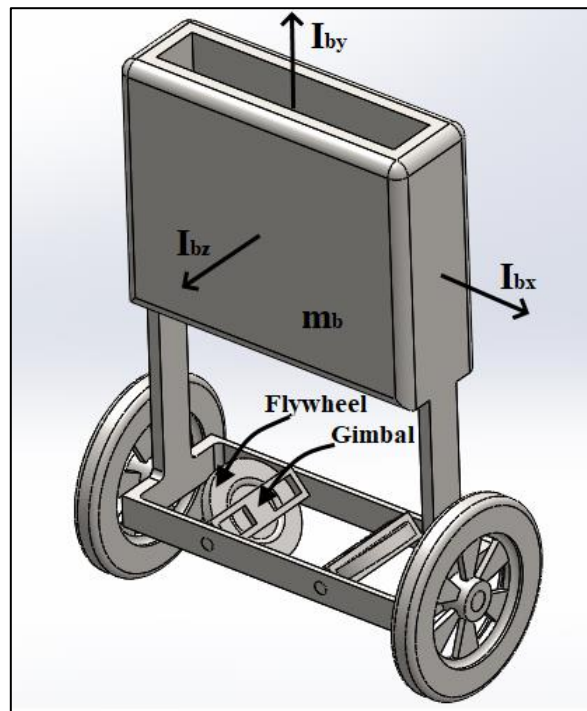

Figure 1. The two-wheeled robot with gyroscopes

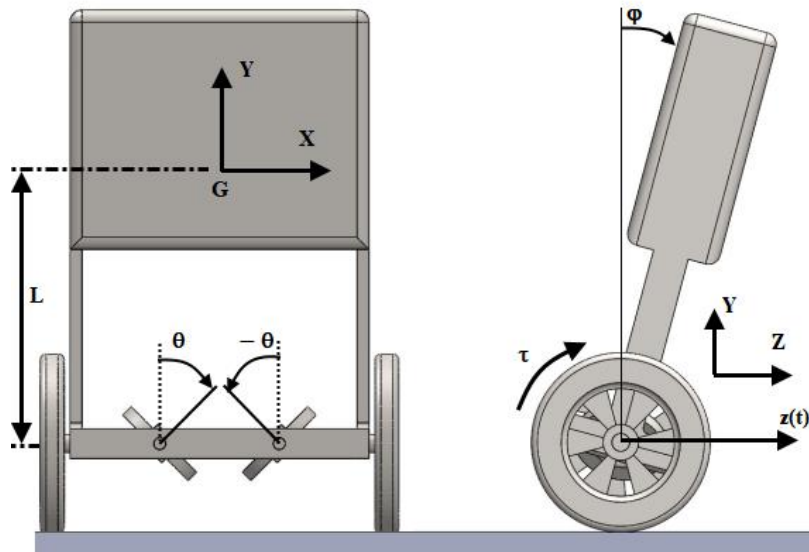**Figure 2.** *Two-wheeled robot with the length of the centroid (G) and head (pitch) displacement (φ) at the free end*

Table 1. *Physical descriptions of the two-wheeled robot*

Symbol	Numerical properties	Definition
g	9.80665 m/s^2	Acceleration due to gravity
r	0.15 m	Radius of the wheel
L	0.47693741 m	Length of the centroid
m_b	169.216910 kg	Body mass
m_g	1.10344600 kg	Gimbal mass
m_w	14.2471463 kg	Wheel mass
m_d	2.52182131 kg	Flywheel mass
I_p	0.00849 $kg.m^2$	Inertia of each flywheel
I_o	0.00432 $kg.m^2$	Inertia of each flywheel
I_{gx}	0.00402 $kg.m^2$	Inertia of each gimbal
I_{gy}	0.00410 $kg.m^2$	Inertia of each gimbal
I_{gz}	0.00049 $kg.m^2$	Inertia of each gimbal
I_{bx}	4.90519 $kg.m^2$	Inertia of body
I_w	0.20413 $kg.m^2$	Inertia of the wheel
Ω	0-3000 rad/s	Flywheel speed
τ	1 N.m	Torque for each wheel

2.1. Equations of Motion

The equations describing the robot motion can be derived by the Lagrange formula. Fortunately, the fundamental equations of the two-wheeled robot using CMG are obtained by Ünker [1] as

$$\left(M_t + \frac{2I_w}{r^2}\right)\ddot{z} + m_b L\ddot{\varphi}\cos\varphi - m_b L\dot{\varphi}^2\sin\varphi = \frac{2\tau}{r}; \tag{1}$$

$$\left(I_o + I_{gz}\right)\ddot{\theta} + \left(I_o - I_p + I_{gx} - I_{gy}\right)\dot{\varphi}^2\cos\theta\sin\theta - I_p\Omega\dot{\varphi}\cos\theta = 0 ; \tag{2}$$

$$\left(2I_o\cos^2\theta + 2I_p\sin^2\theta + 2I_{gx}\cos^2\theta + 2I_{gy}\sin^2\theta + I_{bx} + m_b L^2\right)\ddot{\varphi} + 4\left(I_p - I_o + I_{gy} - I_{gx}\right)\dot{\varphi}\dot{\theta}\sin\theta\cos\theta + 2I_p\Omega\dot{\theta}\cos\theta + \ddot{z}m_b L\cos\varphi - m_b gL\sin\varphi = -2\tau; \tag{3}$$

In which

$$M_t = 2m_d + 2m_g + 2m_w + m_b. \tag{4}$$

2.2. Balance Locations for Small Oscillations

Let's assume that the acceleration of the head motion of the robot is negligible ($\ddot{\varphi}\approx0$) for a low frequency with a small amplitude of the pitch vibrations ($\varphi\approx0$, $\sin\varphi = \varphi$ and $\cos\varphi = 1$). Also, if we make another assumption for the balanced position of the gimbal body, it has zero kinetic energy at a very small precession. ($\theta\approx0$, $\sin\theta = \theta$, and $\cos\theta = 1$). Thus, the equations of the mathematical model of motion can be simplified using $\dot{\theta}\approx0$ and $\dot{\varphi}\approx0$ assumptions in Equations (1), (2), and (3). Hence, ignoring the terms of a higher power of angular velocities at the equilibrium position for a very small amplitude of precession ($\theta\approx0$ $\sin\theta = \theta$, and $\cos\theta = 1$), the differential equations of motion can be simplified to;

$$\left(M_t + \frac{2I_w}{r^2}\right)\ddot{z} = \frac{2\tau}{r}; \tag{5}$$

$$\left(I_o + I_{gz}\right)\ddot{\theta} - I_p\Omega\dot{\varphi} = 0; \tag{6}$$

$$2I_p\Omega\dot{\theta} + \ddot{z}m_b L - m_b gL\varphi = -2\tau. \tag{7}$$

2.3. Required Flywheel Speeds corresponding to the Operating Frequencies

Let the wheels of the robot be stimulated with a harmonic distortion torque as $\tau = \tau_0 e^{j\omega t}$. The displacements of the robot body and gimbal can then be written in terms of angular frequency (ω):

$$z = z_0 e^{j\omega t}, \theta = \theta_0 e^{j\omega t} \text{ and } \varphi = \varphi_0 e^{j\omega t}. \tag{8}$$

Thus, using Equation (8) in Equations (5-7) to solve these reduced equations of motion simultaneously, the following matrix can be written in the form:

$$\begin{bmatrix} -\omega^2\left(M_t + \frac{2I_w}{r^2}\right) & 0 & 0 \\ 0 & -\omega^2(I_o + I_{gz}) & -j\omega I_p\Omega \\ -\omega^2 m_b L & 2j\omega I_p\Omega & -m_b gL \end{bmatrix}\begin{Bmatrix} z_0 \\ \theta_0 \\ \varphi_0 \end{Bmatrix} = \begin{Bmatrix} 2\tau_0/r \\ 0 \\ -2\tau_0 \end{Bmatrix}. \tag{9}$$

From the determinant of the coefficients (z_0, θ_0, and φ_0), the characteristic equation is as follow;

$$\left[(I_o + I_{gz})m_b gL - 2(I_p\Omega)^2\right] = 0. \tag{10}$$

Therefore, Equation (10) can be rearranged into the following flywheel speed resonance;

$$\Omega_{resonance} = \mp\frac{1}{I_p}\sqrt{\frac{(I_o + I_{gz})m_b gL}{2}}. \tag{11}$$

Furthermore, the amplitudes of vibrations can be found from Equation (9) as follows, respectively;

$$z_0 = -\frac{2\tau_0}{\omega^2 r\left(M_t + \frac{2I_w}{r^2}\right)}; \tag{12}$$

$$|\theta_0| = \frac{2\tau_0 I_p\Omega\left[1 + \frac{m_b L}{r\left(M_t + \frac{2I_w}{r^2}\right)}\right]}{-\omega\left[(I_o + I_{gz})gm_b L - 2(I_p\Omega)^2\right]}; \tag{13}$$

$$\varphi_0 = \frac{2\tau_0(I_o + I_{gz})\left[1 + \frac{m_b L}{r\left(M_t + \frac{2I_w}{r^2}\right)}\right]}{(I_o + I_{gz})gm_b L - 2(I_p\Omega)^2}. \tag{14}$$

Thus, the required flywheel speed can be obtained from Equation (13) such as;

$$\Omega_{1,2} = \frac{-b \pm \sqrt{b^2 - 4ac}}{2a}; \tag{15}$$

in which:

$$a = 2\omega|\theta_0|I_p^2 ;$$

$$b = -2\tau_0 I_p \left[1 + \frac{m_b L}{r\left(M_t + \frac{2I_w}{r^2}\right)} \right];$$ (16)

$$c = -\omega |\theta_0| g m_b L \left(I_o + I_{gz} \right).$$

The lowest flywheel speed that can be used versus a required precession amplitude θ_0 can be determined by the equations obtained above. Equations (13 and 14) illustrate that the amplitudes increase when the wheel's torque increases, which means more inertia force for the body of the robot in the horizontal axis. The curves in Figure 3 are plotted with the help of these equations derived above. As the frequency increases, the amplitude of the body vibration increases. It is necessary to increase the flywheel speed at low-frequency values as seen in Figure 3. Therefore, low angular momentum is needed at high roll amplitudes of gyro, according to the relationship between the flywheel speed and the roll amplitude.
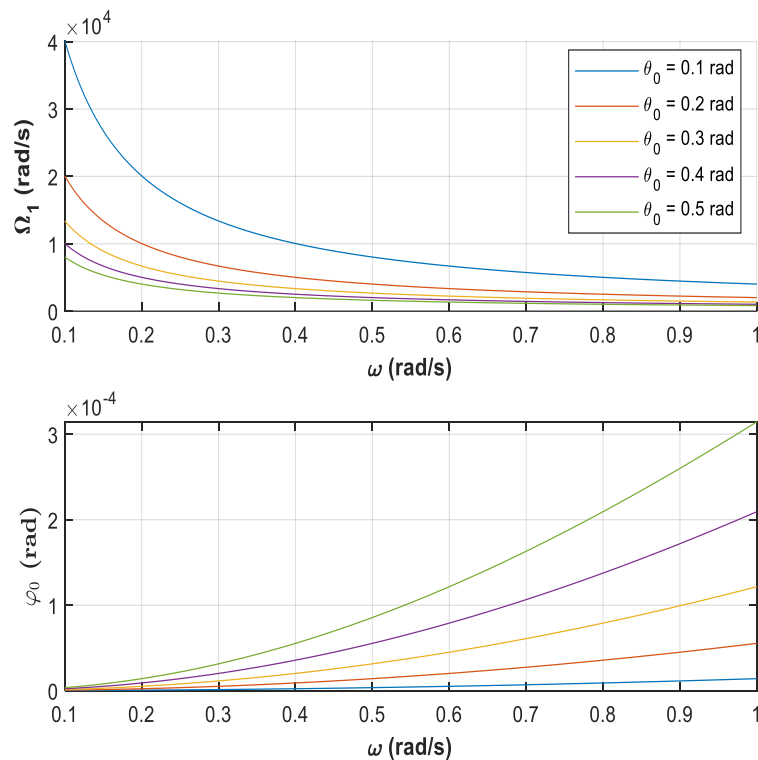

Figure 3. *The frequency influence on the flywheel speed, Ω and the pitch amplitude, φ_0 for $\tau_0 = 1$ Nm*

3.RESULTS AND DISCUSSION

In this study, Lagrangian equations are solved with the help of MATLAB. The physical parameters to be used in solving the equations of motion of the model are given in Table 1. Numerical solutions of model equations were run for 0.05 s step intervals. The theoretical simulations of equations of motion were confirmed with the simulations obtained by ANSYS for different speeds of flywheels. The displacements are obtained by the Rigid Dynamics tool of ANSYS Workbench.

3.1. Influence of the Angular Frequencies

The oscillation amplitudes obtained from the flywheel speed scanning are shown in Figure 4. In which, the flywheel speed of the CMG saves the robot from instability as soon as it reaches a certain speed. For example, for this model, the required speed is $\Omega=1000$ rad/s, after which the robot moves stably and

protects itself with gradually decreasing vibration amplitude. In addition, by increasing the flywheel speed of the gyro, the amplitudes for each frequency can be reduced to desired levels.

In Figure 5, the optimum flywheel speed calculated using Equation (15) to minimize the oscillation amplitude of the target frequency at values of $\tau_0 = 1$ Nm and $\theta_0 = 0.3$ rad is 2688 rad/s. As can be seen from Figure 5, significant decreases were observed in the amplitudes of the vibrations, as the required flywheel speed would decrease as the frequency increased. Consequently, for the same angular momentum, the vibration amplitudes gradually increase as the frequency decreases.
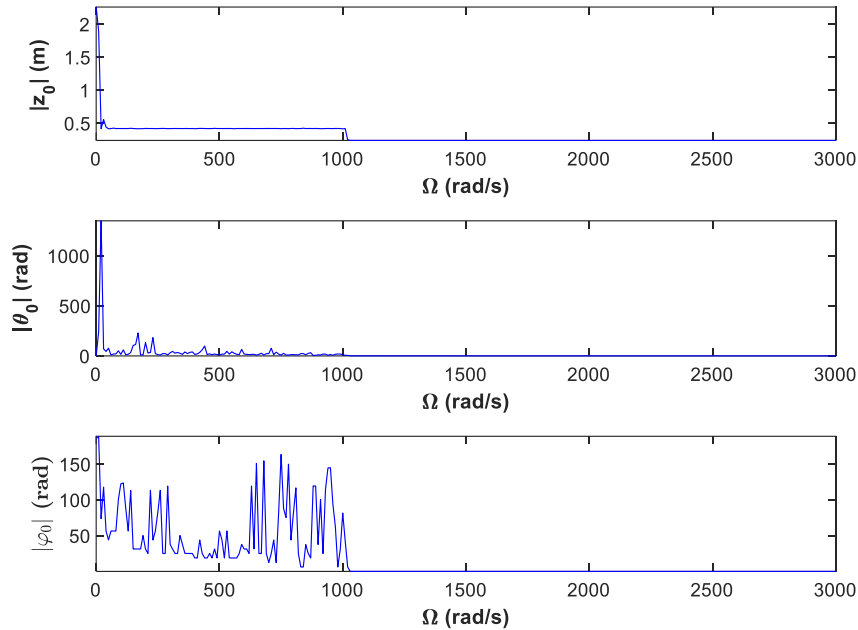

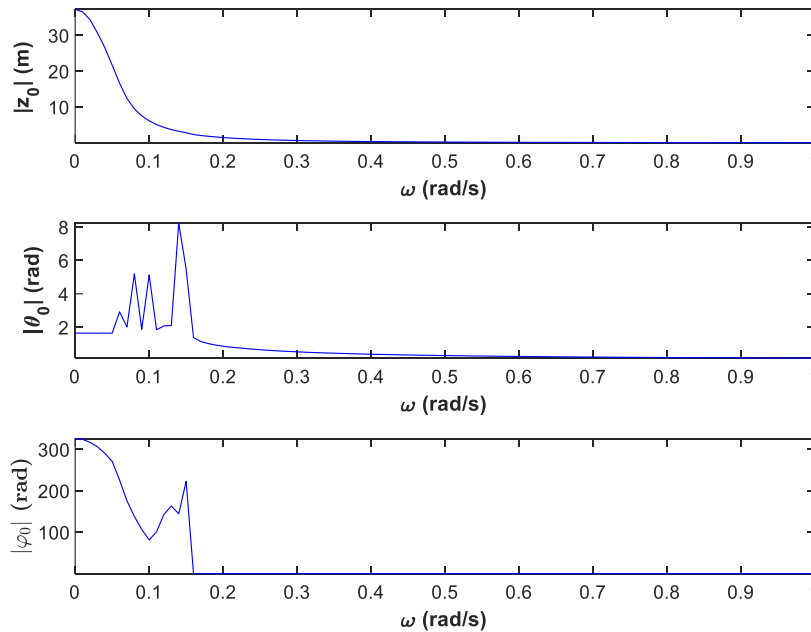**Figure 4.** *Influence of the flywheel speed Ω for $\tau_0 = 1$ Nm and $\omega=0.5$ rad/s*

Figure 5. *Influence of the angular frequency ω for $\tau_0 = 1$ Nm and $\Omega = 2688$ rad/s*

3.2. Comparisons of Ansys and the Theoretical Results

It can be seen from the comparisons that the results of the displacements agreed well and the simulations of ANSYS and the theoretical results are almost the same as provided in Figures 6 - 8. By increasing the gimbal amplitude, the required flywheel speed can be reduced. This means less angular momentum is needed for the robot's balance. The damping performance of the CMG was achieved by using low flywheel speed at large gimbal amplitude. However, in this case, it caused the oscillation amplitude of the robot body to increase. The oscillation amplitudes in Figure (3), plotted with the aid of Equation (15), contain minor errors due to the linearized equations. While a gyro's flywheel is rotating at a certain constant speed, the gimbal and body oscillate for the stability of the robot. That is, for the same preventing rollover performance, the required flywheel speed can be reduced if a higher roll amplitude of the gyro is used, taking into account the stability of the robot.
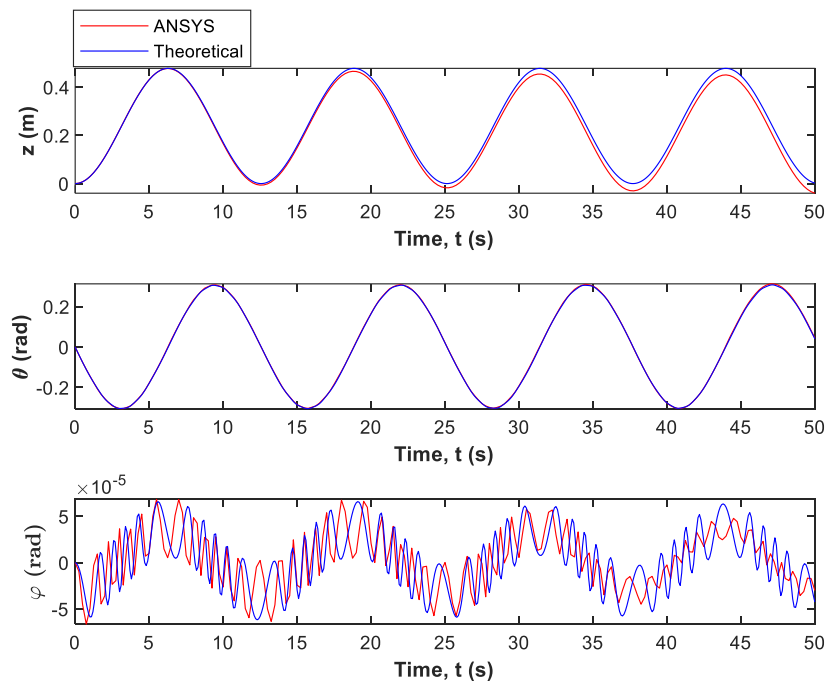

Figure 6. *Comparison of ANSYS software and the theoretical results with the frequency $\omega=0.5$ rad/s, $\Omega = 2688$ rad/s, and $\tau_0 = 1$ Nm for $\theta_0=0.3$ rad*
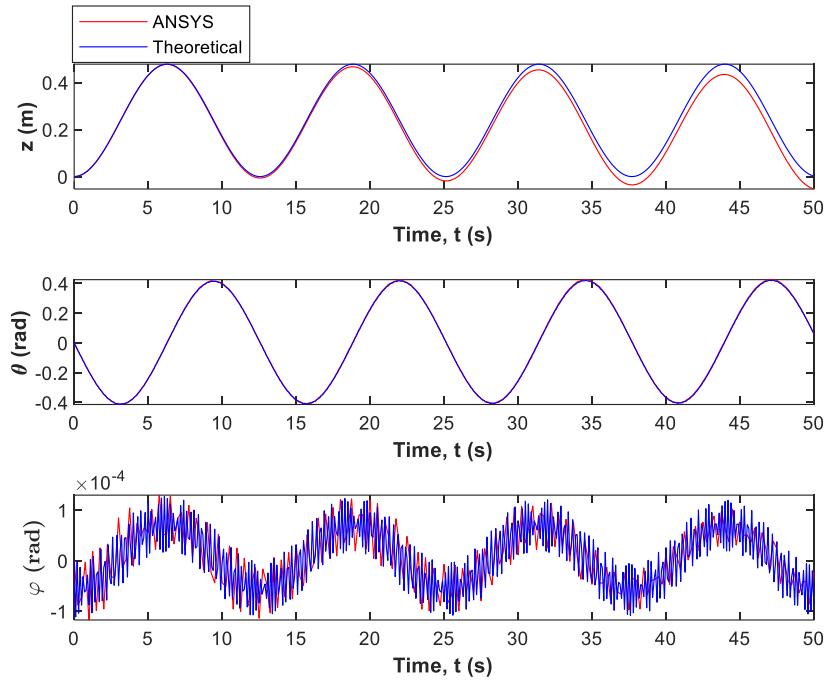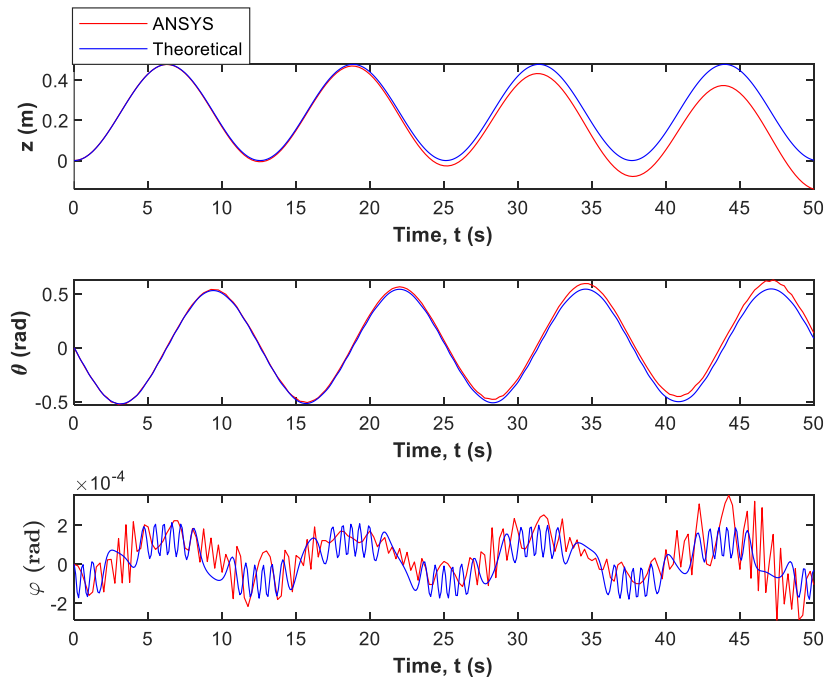
Figure 7. *Comparison of ANSYS software and the theoretical results with the frequency ω=0.5 rad/s, Ω = 2022 rad/s, and τ₀ = 1 Nm for θ₀=0.4 rad*

Figure 8. *Comparison of ANSYS software and the theoretical results with the frequency ω=0.5 rad/s, Ω = 1623 rad/s, and τ₀ = 1 Nm for θ₀=0.5 rad*

4.CONCLUSIONS

In this study, the nonlinear dynamic equations of the robot with CMG were obtained using the Lagrangian approach. In addition, a CAE software (ANSYS) model was tested to check the damping capability of the GMG. As a result, it is seen that Lagrange model and ANSYS simulations are similar.

CMG can convert the angular momentum to unidirectional thrust at the center of body mass along the forcing excitation axis, which has considerably attenuated the vibration at the target frequency. However, the system becomes unstable when descending to low excitation frequencies at a constant speed of the flywheel. Since stability is dependent on angular momentum, damping performance improved as the flywheel speed of the gyroscope increased. This article demonstrates that there is a correlation between the flywheel speed and the gimbal's precession amplitude. Namely, when a high roll amplitude is used, the required angular momentum can be reduced for damping.

ACKNOWLEDGEMENTS

REFERENCES

[1] Ünker, F. (2022). Proportional control moment gyroscope for two-wheeled self-balancing robot. Journal of Vibration and Control, 28 (17-18), 2310–2318. https://doi.org/10.1177/10775463211009988

[2] Nghia, V.B.V., Van Thien, T., Son, N.N., & Long, M.T. (2022). Adaptive neural sliding mode control for two wheel self balancing robot. Int. J. Dynam. Control, 10, 771–784. https://doi.org/10.1007/s40435-021-00832-1

[3] Chan, R.P.M., Stol, K.A., & Halkyard, C.R. (2013). Review of modelling and control of two-wheeled robots. Annual Reviews in Control, 37 (1), 89–103. https://doi.org/10.1016/j.arcontrol.2013.03.004

[4] Alqudsi ,Y.Sh., Dorrah, H. T., Kassem, A. H., & El-Bayoumi, G. M. (2022). Robust compound control for wheeled inverted pendulum in an uncertain and disturbed environment. Engineering Science and Technology, an International Journal, 28, 101024. ISSN 2215-0986, https://doi.org/10.1016/j.jestch.2021.06.004.

[5] Abut, T., & Soyguder, S. (2022). Two-loop controller design and implementations for an inverted pendulum system with optimal self-adaptive fuzzy-proportional–integral–derivative control. Transactions of the Institute of Measurement and Control, 44(2), 468-483. https://doi.org/10.1177/01423312211040301

[6] Grasser, F., Arrigo, A.D., & Colombi, S. (2002). JOE: A mobile, inverted pendulum. IEEE Transactions on Industrial Electronics, 49(1), 107–114.

[7] Takei, T., Imamura, R., & Yuta, S. (2009). Baggage transportation and navigation by a wheeled inverted pendulum mobile robot. IEEE Transactions on Industrial Electronic, 56(10), 3985-3994.

[8] Larimi, S.R., Zarafshan, P., & Moosavian, S.A.A. (2015). A New Stabilization Algorithm for a Two-Wheeled Mobile Robot Aided by Reaction Wheel. Journal of Dynamic Systems, Measurement, and Control, 137(1), 011009 (8 pages).

[9] Çuvalcı, O., Ünker, F., Baturalp, T. B., Gülbulak, U., & Ertaş, A. (2021). Modal Control of Cantilever Beam Using a Gyrostabilizer. Sound & Vibration, 55(4), 281—294. https://doi.org/10.32604/sv.2021.015705

[10] Ünker, F., & Çuvalcı, O. (2019). Optimum Tuning of a Gyroscopic Vibration Absorber for Vibration Control of a Vertical Cantilever Beam with Tip Mass. International Journal of Acoustics and Vibration, 24(2), 210–216. https://doi.org/10.20855/ijav.2019.24.21158

[11] Ünker, F. (2020). Tuned gyro pendulum stabilizer for control of vibrations in structures. International Journal of Acoustics and Vibration, 25(3), 355–362. https://doi.org/10.20855/ijav.2020.25.31632

[12] Oueini, S., Nayfeh, A., & Pratt, J. (1999). A review of development and implementation of an active nonlinear vibration absorber. Archive of Applied Mechanics, 69, 585–620. https://doi.org/10.1007/s004190050245